Quantum well structure of a double perovskite superlattice and formation of a spin-polarized two-dimensional electron gas

S. Samanta, S. B. Mishra, and B. R. K. Nanda*

Condensed Matter Theory and Computational Lab, Department of Physics, Indian Institute of Technology Madras, Chennai 600036, India

(Received 15 February 2018; revised manuscript received 22 June 2018; published 26 September 2018)

Layered oxide heterostructures are the new route to tailor desired electronic and magnetic phases emerging from competing interactions involving strong correlation, orbital hopping, tunneling, and lattice coupling phenomena. Here, we propose a half-metal/insulator superlattice that intrinsically forms a spin-polarized two-dimensional electron gas (2DEG) following a mechanism very different from the widely reported 2DEG at the single perovskite polar interfaces. From a density functional theory plus U study on a Sr_2FeMoO_6/La_2CoMnO_6 (001) superlattice, we find that a periodic quantum well is created along [001] which breaks the threefold t_{2g} degeneracy to separate the doubly degenerate xz and yz states from the planar xy state. In the spin-down channel, the dual effect of quantum confinement and strong correlation localizes the degenerate states, whereas the dispersive xy state forms the 2DEG, which is robust against perturbations to the superlattice symmetry. The spin-up channel retains the bulk insulating. Both spin polarization and orbital polarization make the superlattice ideal for spintronic and orbitronic applications. The suggested 2DEG mechanism widens the scope of fabricating the next generation of oxide heterostructures.

DOI: 10.1103/PhysRevB.98.115155

I. INTRODUCTION

Channelizing the electronic motion through confinement is the key to the future success of fabrication of nanoscale electronic devices [1]. One of the most appropriate ways of achieving this is to tailor the potential profile of electrons by constructing heterointerfaces [2], superlattices [3], and thin films [4], where the confinement length is comparable to the de Broglie wavelength of the associated electron. Among the heterostructures and films, the oxide families are intriguing and exhibit novel quantum states due to collective phenomena by virtue of the interplay between spin, charge, and orbital degrees of freedom [5–7].

The widely investigated insulating oxide interfaces $LaAlO_3/SrTiO_3$ [8–10] and $LaMnO_3/SrMnO_3$ [11,12] produce a two-dimensional electron gas (2DEG) to quench the polar catastrophe that arises due to alternate stacking of positively and negatively charged layers along the La side and charge-neutral layers along the Sr side. A 2DEG can also be formed by quantizing the three-dimensional metallic state through a confinement potential. While examples are many in semiconducting heterostructures [13,14], it is a rare occurrence in the family of correlated oxides. One of them is the case of the $SrVO_3$ ultrathin film (eight monolayers) deposited on the $Nb:SrTiO_3$ substrate [4]. Here, the three-dimensional metallic V t_{2g} states are confined by the potential well which is formed due to the Schottky barrier created at the $Nb:SrTiO_3/SrVO_3$ interface and the natural barrier at the $SrVO_3$/vacuum interface. Such orbital-selective quantization by exploiting the d-orbital anisotropy forms the basic premise for the evolving area of orbitronics [15], where the electric currents are controlled through d-orbital states [16]. The natural extension of orbitronics is to spin polarize the preexisting conducting electrons by exploiting the spin anisotropy, which is one of the primary intents of this work.

To begin with, it is essential to have a source of spin-polarized conducting electrons, and in this context, the double perovskite Sr_2FeMoO_6 (SFMO) has already been well established as a half-metallic system with high Curie temperature ($T_C \sim 450$ K) [17] and spin polarization as large as 70% [18]. The dispersive Mo 4d (xy, xz, and yz) states are partially occupied in the spin-down channel, while a large band gap exists in the spin-up channel to create a half-metallic system where the electrons are mobile in all three dimensions. A quantum well structure can be designed to quantize the SFMO mobile electrons by tailoring a bicolor superlattice with the other constituent being an insulator. The rare ferromagnetic insulator La_2CoMnO_6 (LCMO) is an excellent choice as its T_C is close to 230 K [19,20], and it offers a minor in-plane lattice mismatch ($\sim$1.5%) when the superlattice is grown along the [001] direction.

Recent advances in modern state-of-the-art techniques such as molecular beam epitaxy and atomic layer deposition methods have paved the way to create such layered oxide superlattices. Stable nanometer-thick SFMO and LCMO films, grown using pulse laser deposition (PLD) and RF magnetron sputtering techniques, have already been reported in the literature [21–24]. Also, experimentally, successful attempts have been made to grow freestanding oxide films (e.g., VO_2 [25], Fe_3O_4 [26], $Pb(Zr, Ti)O_3$ [27], and interfaces $BiFeO_3/CoFe_2O_4$ [28]) using van der Waals heteroepitaxy techniques.

In this work, we examine the $(SFMO)_2/(LCMO)_2$ superlattices in two different configurations, as shown in Fig. 1, using density functional theory (DFT) plus U calculations.

*nandab@iitm.ac.in

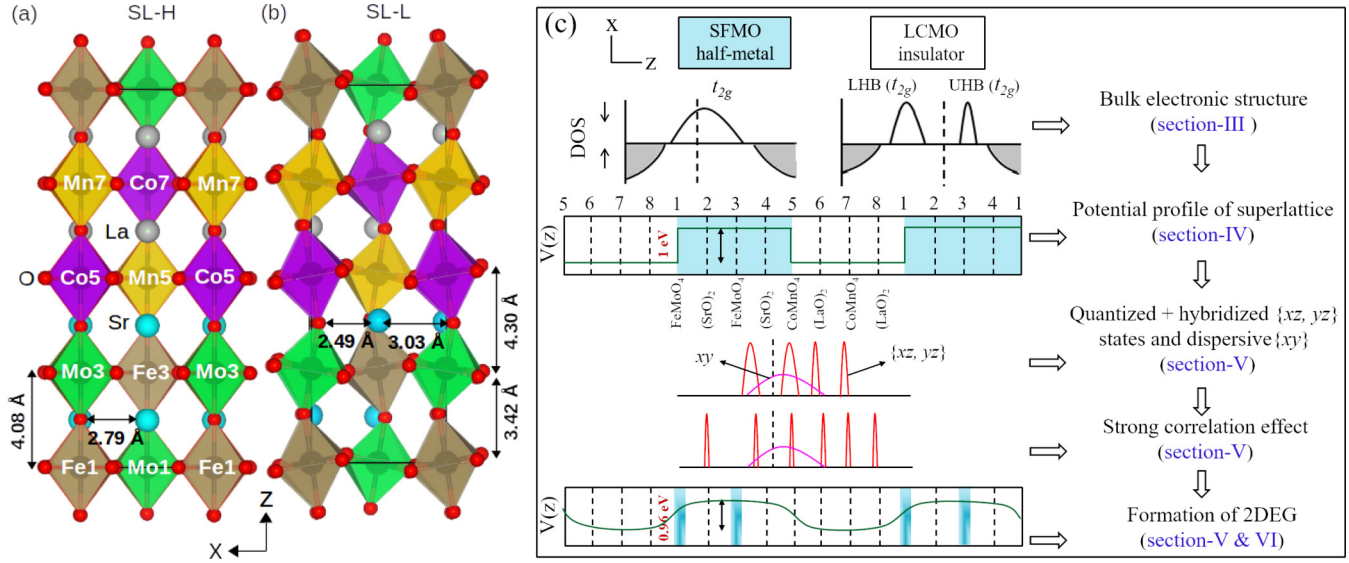

FIG. 1. Crystal structure of the $(SFMO)_2/(LCMO)_2$ superlattice and the mechanism for formation of a 2DEG. (a) The $(SFMO)_2/(LCMO)_2$ superlattice assuming highly symmetric SFMO as the substrate (SL-H). (b) The same superlattice, but with lower symmetric LCMO as the substrate (SL-L). The lowering in the symmetry of the SL-L superlattice is due to the tilting and rotation of the octahedral complexes. (c) Schematic illustration of quantum confinement and the formation of a spin-polarized two-dimensional electron gas in the superlattices. Here, the up arrow and down arrow represent the spin-up and spin-down DOSs, respectively, and t_{2g} denotes the triply degenerate (xy, yz, xz) states. In SFMO, it carries the character of Fe and Mo d states, signifying stronger Fe-Mo hybridization. In LCMO, the strong correlation effect splits the Co t_{2g} states to form two subbands, namely, the lower Hubbard band (LHB) and upper Hubbard band (UHB). The potential well of the superlattice breaks the threefold degeneracy into twofold degenerate xz and yz states and a nondegenerate xy state. While the former are quantized, the latter remains dispersive as in the bulk to form the 2DEG.

In the first case, assuming the higher-symmetry tetragonal SFMO as the substrate, the in-plane symmetry of the superlattice is taken to be the same as that of SFMO, and we define the structure as SL-H. The second configuration (SL-L) carries the in-plane symmetry of lower-symmetry monoclinic LCMO. In both configurations, the atomic positions are relaxed to obtain the ground state.

The electronic and magnetic ground states of both SL-H and SL-L superlattices reveal no new magnetic ordering. However, a periodic quantum well with depth close to 1 eV develops along the z axis (growth direction) due to the difference in the chemical potentials of the constituents. As a consequence, there is an orbital-selective quantization of the fractionally occupied t_{2g} itinerant states. The strong correlation further localizes these quantized states. During the whole process the planar xy dispersive state remains unchanged, which leads to the evolution of a two-dimensional spin-polarized electron gas (2D-SPEG) from a three-dimensional (3D) SPEG. The mechanism, as understood from the electronic structure calculations presented in this paper, is schematically illustrated in Fig. 1. It completely differs from the mechanism of charge reconstruction involved in single perovskite polar interfaces and hence opens up new avenues to synthesize next-generation heterostructures out of nonpolar correlated oxides in order to create a 2DEG for practical purposes.

II. COMPUTATIONAL DETAILS

DFT calculations are carried out using both the pseudopotential method with the plane-wave basis set as implemented in the QUANTUM ESPRESSO simulation package [29] and the full-potential linearized augmented plane-wave method with the basis set including local orbitals (FP-LAPW+lo) as implemented in the WIEN2K simulation package [30]. For both cases the Perdew-Burke-Ernzerhof generalized gradient approximation (GGA) [31] exchange-correlation functional is considered, and an $8 \times 8 \times 8$ Monkhorst-Pack k mesh is used for the Brillouin zone integration.

The pseudopotential method is used for structural optimization and for the calculation of the electrostatic potential in the real space. For structural relaxation, the kinetic energy cutoff for the plane waves is set to 30 Ry. The electron-ion interaction is considered within the Vanderbilt ultrasoft pseudopotential for which charge density cutoff is chosen to be 300 Ry. The tolerance for the Hellmann-Feynman force on each atom is taken to be 20 meV/Å.

The optimized structure obtained from the pseudopotential method has been further used for the calculation of electronic and magnetic structures using the FP-LAPW method. The computational details for this method are as follows. To incorporate the effect of strong correlation, an effective on-site correlation parameter U ($U_{\text{eff}} = U - J$) is included through the rotationally invariant Dudarev approach [32]. All the results in the paper are presented for $U = 3$ eV. However, to examine the invariance of the mechanism, the results are also analyzed for higher U ($= 5$ eV). The LAPW basis function considers $5d$ and $6s$ of La; $5s$ of Sr; $3d$ and $4s$ of Mn, Fe, and Co; $4d$ and $4s$ of Mo; and $2s$ and $2p$ of O. RK_{max} is taken to be 7.0, yielding 24235 plane waves for each k point in the interstitial region. The principal components of conductivity tensors $\sigma_{\alpha\beta}$ are computed using semiclassical Boltzmann transport theory

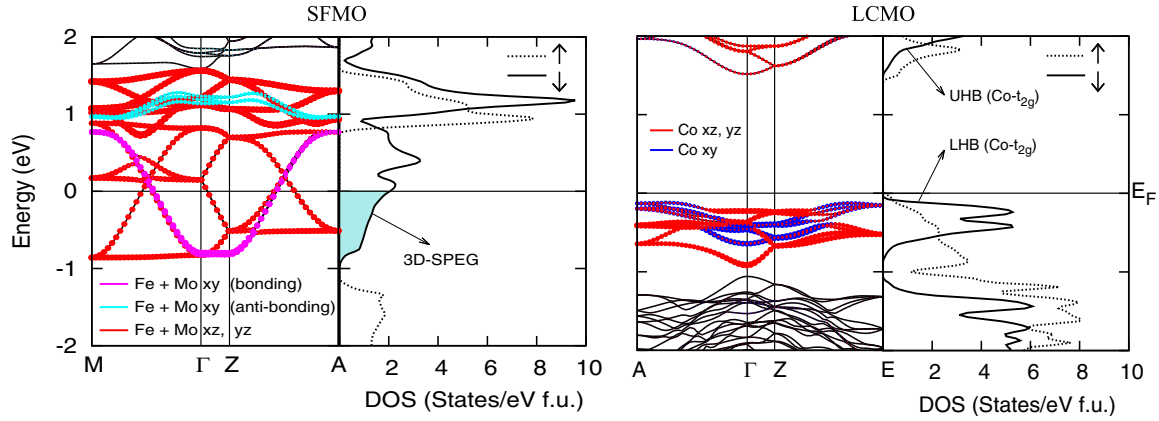

FIG. 2. Band structure (shown in the spin-down channel) and densities of states for SFMO and LCMO. The results are obtained using GGA + U ($U = 3$ eV). A four-formula unit cell is used in order to have a Brillouin zone identical to that of the superlattice. The partially occupied t_{2g} states in the spin-down channel form the 3DEG. LCMO exhibits an insulating ground state following Mott mechanism.

as implemented in the BOLTZTRAP code [33]. A highly dense nonshifted mesh with 32000 k points is used to obtain the smooth interpolation of bands and to compute the necessary derivatives which are required for the calculation of $\sigma_{\alpha\beta}$.

III. BULK ELECTRONIC STRUCTURE

Bulk SFMO is a half-metallic ferrimagnet, where only the spin-down channel exhibits the metallic behavior and Fe spins are aligned antiparallel to Mo spins [17,34]. As Fig. 2 shows, the Fermi level E_F in the spin-down channel is occupied by the Mo predominant bonding states of the Mo $t_{2g}\downarrow$-Fe $t_{2g}\downarrow$ hybridization. In the d^5 configuration of the high-spin Fe^{3+} ion, the $t_{2g}\downarrow$ state is expected to be empty. Similarly, in the d^1 configuration of the Mo^{5+} ion, the $t_{2g}\downarrow$ state is partially occupied, while the $d\uparrow$ states are empty. However, the delocalized $4d$ states hybridize significantly with the Fe $t_{2g}\downarrow$ states to form a set of partially occupied dispersive bands. As a consequence, a three-dimensional spin-polarized electron gas is formed.

Double perovskite LCMO is a rare ferromagnetic insulator [35]. Its band structure and densities of states (DOSs) are shown in Fig. 2. While Mn stabilizes in the 4+ charge state, leading to the $t_{2g}^3\uparrow\ e_g^0\uparrow\ t_{2g}^0\downarrow\ e_g^0\downarrow$ configuration, Co stabilizes in the 2+ charge state, leading to the $t_{2g}^3\uparrow\ e_g^2\uparrow\ t_{2g}^2\downarrow\ e_g^0\downarrow$ configuration. In the spin-up channel, the band gap is opened by the large crystal field split of the Mn d state as well as the large spin-exchange split of both Mn and Co d states [36]. In the absence of a strong correlation effect, the $t_{2g}^2\downarrow$ configuration will create a metallic state for the perfect cubic phase. However, with tilting of the octahedra as well as a strong correlation effect, the t_{2g} states are further split into an occupied lower Hubbard band and an unoccupied upper Hubbard band to open up a gap in the spin-down channel to make the system insulating [37]. Our estimated exchange energies ($J = E_{\uparrow\downarrow} - E_{\uparrow\uparrow}$) confirm that there is a strong ferromagnetic coupling between the Co and Mn spins ($J_{Co-Mn} \sim 10.11$ meV) [38] which overcomes the Co-Co ($J_{Co-Co} \sim -1.92$ meV) and Mn-Mn ($J_{Mn-Mn} \sim -1.52$ meV) antiferromagnetic couplings. The detailed mechanisms are illustrated in the Appendix A to further elucidate the half-metallic and ferromagnetic-insulating behaviors of SFMO and LCMO, respectively.

IV. FORMATION OF A PERIODIC QUANTUM WELL STRUCTURE

The growth of the $(SFMO)_2/(LCMO)_2$ superlattice, as shown in Fig. 1, brings a potential mismatch between the SFMO and LCMO sites and hence creates a quantum well structure. To demonstrate it, we have estimated the variation of the macroscopic average of the electrostatic potential V^{MA} of bulk SFMO and LCMO as well as that of the SL-H superlattice as follows. First, the xy planar average of the potential V^{PA} is obtained by averaging the raw three-dimensional potential V^{raw} [39]:

$$V^{PA}(z) = \frac{1}{S}\int_s V^{\text{raw}}(x, y, z)dxdy, \tag{1}$$

where S is the area of the (001) plane of the unit cell. V^{PA} is further averaged to obtain V^{MA}:

$$V^{MA}(z) = \frac{1}{c}\int_{z-c/2}^{z+c/2} V^{PA}(z')dz'. \tag{2}$$

Here, c is the length of one period. For LCMO and SFMO slabs, the respective lattice parameters are taken as c. In the case of a superlattice, V^{MA} is calculated using the c lattice parameter of SFMO as well as that of LCMO, and the average of the two is considered to minimize the error at the interface [40].

Figure 3 shows V^{PA} and V^{MA} for the pure LCMO and SFMO slabs as well as for the SL-H superlattice. When compared with the vacuum level, V^{MA} of the SFMO slab is found to be ~1 eV higher than that of the LCMO side. Hence, in the absence of any significant ionic displacements and breakdown of the planar geometry, the SL-H superlattice is expected to produce a periodic quantum well structure with a depth of 1 eV. Our structural relaxation on the SL-H superlattice suggests that nonplanar displacement of the ions is of the order of 0.004 Å, and therefore, the layered geometry is maintained. Also, Fig. 3(b) infers that V^{MA} of

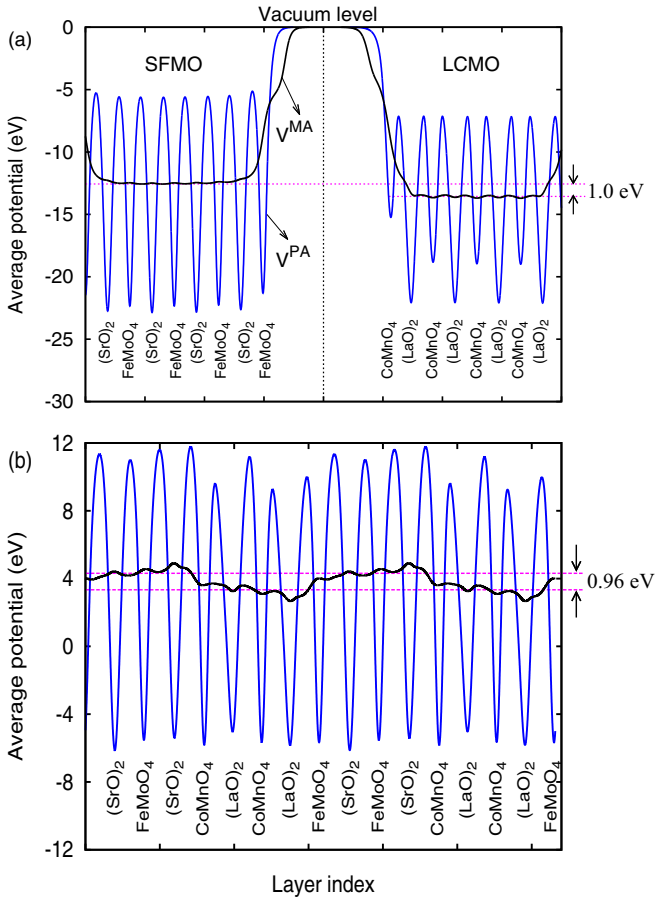

FIG. 3. (a) Planar average (V^{PA}) and macroscopic average (V^{MA}) potentials of four-unit-cell-thick SFMO and LCMO slabs with reference to the vacuum level. (b) V^{PA} and V^{MA} of the SL-H superlattice suggesting the formation of a periodic quantum well structure.

the superlattice in the ground-state structure shows a periodic quantum well with a depth of ∼0.96 eV.

The spin-polarized 3DEG of the superlattice will now experience this periodic quantum well and also the strong correlation effect. Hence, new quantum states are expected to emerge which we have examined by carrying out band structure calculations.

V. EIGENSTATE RECONSTRUCTION AND FORMATION OF A 2DEG

In the spin-up channel, bulk SFMO and LCMO exhibit a band gap larger than the depth of the potential well (see Fig. 2). Therefore, in this spin channel, like the bulk, the superlattices also exhibit insulating behavior. Hence, our band structure analysis for the superlattice is restricted to the spin-down channel.

The t_{2g} projected spin-down band structure of the SL-H superlattice within the independent electron approximation ($U = 0$) is shown in Fig. 4. Since Mn $t_{2g} \downarrow$ states lie far above E_F due to large exchange splitting, the effect of the potential well is inconsequential. For the remaining six transition-metal elements (two of each of Fe, Mo, and Co), the periodic

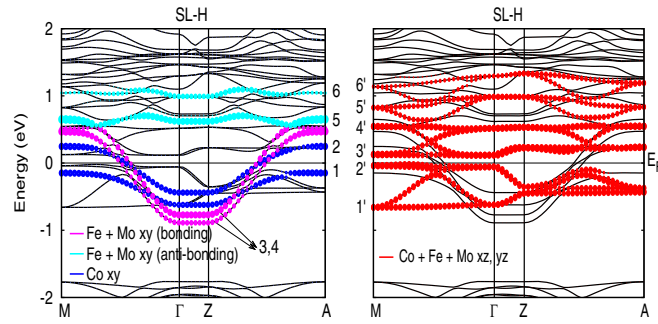

FIG. 4. Spin-down band structure of the SL-H superlattice for $U = 0$. The contributions of the planar orbitals (Mo, Fe, and Co xy) and the z-axis-oriented orbitals (xz and yz) to the band structure are shown on the left and the right, respectively. The discrete pairs $1'$ to $6'$ are the outcome of the quantization through the periodic potential well (see Fig. 3). The partially occupied bands, 3 and 4 in the left panel, form the spin-polarized 2DEG.

potential well along z breaks the threefold degeneracy and splits the corresponding $t_{2g} \downarrow$ states into planar xy and twofold-degenerate xz and yz states. The left panel of Fig. 4 highlights the xy-orbital-dominated bands. The two lower-lying (nearly) occupied parabolic bands (1, 2; blue) belong to two Co atoms located in the lower potential region. Out of the remaining four, two of them are partially occupied parabolic bonding bands (3, 4; magenta), and two of them are the unoccupied antibonding bands (5, 6; cyan) resulting from Fe-Mo $t_{2g} \downarrow - t_{2g} \downarrow$ interactions as discussed for the bulk band structure (Fig. 2). Except for a minor shift in their energy levels, these bonding bands resemble that of the bulk ($U = 3$ eV) band structure, which suggests that these states are delocalized and are not affected by the quantum well.

The right panel of Fig. 4 highlights the bands dominated by the orbitals (xz, yz). Unlike the bands with in-plane xy states, these bands, lying in the range $E_F - 0.8$ to $E_F + 1.2$ eV, are found to be localized and discrete, which is a signature of quantization. Due to the degeneracy of the xz and yz states,

TABLE I. Total energy of different magnetic configurations of the superlattice. In bulk magnetic ordering, the spins of the transition-metal cations in SFMO are antiparallel, whereas they are parallel in LCMO. In the C-AFM configuration, the intraplane coupling between the neighboring spins is antiferromagnetic, while interplane coupling is ferromagnetic. In the G-AFM spin arrangement, both intra- and interplane couplings between the neighboring spins are antiferromagnetic. The A-AFM arrangement corresponds to intraplane ferromagnetic coupling and interplane antiferromagnetic coupling. We find that there are no new magnetic phases, and the superlattice inherits the spin arrangement of the respective bulk compounds.

	Interface magnetic orderings	ΔE (eV)	
		SL-H	SL-L
Bulk	$(Co)_\uparrow(Mn)_\uparrow/(Fe)_\uparrow(Mo)_\downarrow$	0	0
C-AFM	$(Co)_\uparrow(Mn)_\downarrow/(Fe)_\uparrow(Mo)_\downarrow$	0.82	0.19
G-AFM	$(Co)_\uparrow(Mn)_\downarrow/(Fe)_\downarrow(Mo)_\uparrow$	0.73	0.20
A-AFM	$(Co)_\uparrow(Mn)_\uparrow/(Fe)_\downarrow(Mo)_\downarrow$	0.09	0.10

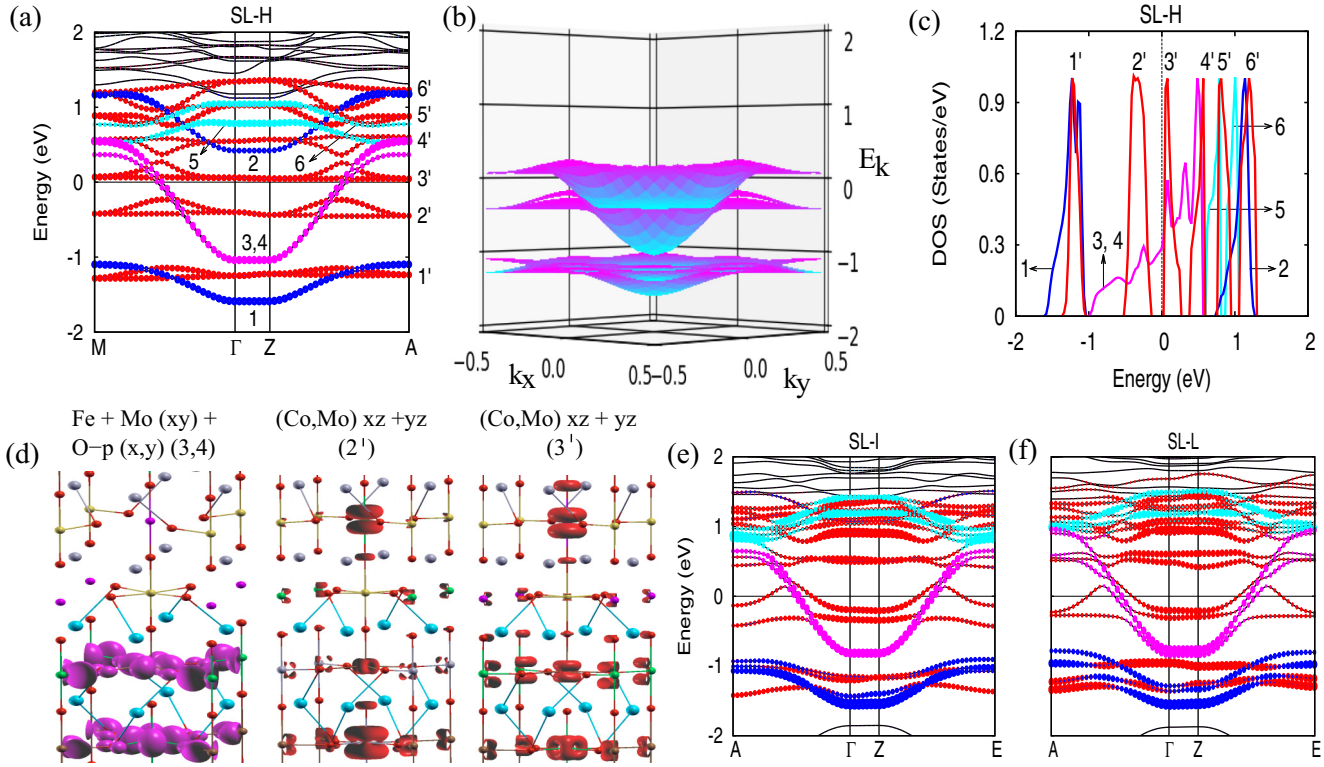

FIG. 5. Strongly correlated electronic structure of the SFMO/LCMO superlattice. (a) The spin-down band structure of the SL-H superlattice projecting the contribution of in-plane (xy) and out-of-plane (xz, yz) orbitals on the bands as obtained using GGA + U (= 3 eV). For the color code of the bands, refer to Fig. 4. (b) The same spin-down band structure, but now plotted in the interfacial reciprocal space (k_x-k_y) plane and in the vicinity of E_F. (c) The spin-down DOS of the SL-H superlattice. The numbering of the bands is identified with discretization due to the effect of both the periodic quantum well and strong correlation. (d) From left to right, the charge density plots for the dispersive bands {3, 4} and quantized bands 2′ and 3′. The former further confirms that the itinerant electrons, occupied by the hybridized states, are formed by the xy, x, and y orbitals of the $FeMoO_4$ plane. The charge densities also reverify that the quantized bands 2′ and 3′ are formed by the out-of-plane xz and yz orbitals. (e) and (f) The spin-down band structure for the superlattices with intermediate symmetry (SL-I) and with lower symmetry (SL-L) [see Fig. 1(b)], respectively. While the lowering in symmetry further discretizes the quantized bands, the partially occupied dispersive bands {3, 4} are almost unaffected.

there are six pairs of such bands (1′ to 6′ in Fig. 4, right). The lower, middle, and upper two pairs are predominantly contributed by Co, Fe, and Mo atoms, respectively. However, the reasonable presence of Mo {xz, yz} characters in the lower two pairs suggests that a new Mo t_{2g}-Co t_{2g} hybridization has taken place across the interface.

The independent electron approximation does not provide the exact ground state, particularly in the case of oxides, as there is inadequacy in accounting for the electron correlation in the system. The correlation effect can be included through the parametric Hubbard U formalism. As the ground-state electronic structure of bulk SFMO and LCMO is accurately estimated for $U = 3$ eV, we have considered the same for the superlattices as well. Also, to determine the ground-state magnetic configuration, several possible arrangements of the Co, Mn, Fe, and Mo spins are considered, and the corresponding total energies are estimated in Table I. We find that there is no magnetic reconstruction, and the bulk magnetic ordering of SFMO and LCMO constitutes the magnetic ground state of the superlattice.

The spin-down band structure for the magnetic ground state of the SL-H superlattice is shown in Fig. 5(a). We find that following the Mott mechanism, there is a significant re-positioning of the bands with respect to the $U = 0$ band structure. Out of the two lower-lying Co xy-dominated bands (1 and 2 in Fig. 4, left), the occupied one lowers its energy by roughly 1 eV, and the fractionally occupied one raises its energy by approximately 1 eV to become unoccupied. However, the fractionally occupied itinerant Mo-Fe bonding xy states remain unchanged. Similarly, in the case of potential well quantized bands, dominated by xz, yz characters, the lowest pair (1′) is pushed down further below and lies at −1.2 eV with respect to E_F. Also, there is a visible separation of 0.5 eV between the next two quantized pairs (2′ and 3′). While 2′ is completely occupied, 3′ is empty. These two quantized states are now dominated by Mo and Co xz, yz characters. The upper three quantized states are less affected by the U effect. In addition to the repositioning, the strong correlation effect further localizes the quantized states. The band dispersion, plotted in the interfacial reciprocal space [$k_x - k_y$ plane; Fig. 5(b)], and the eigenstate-resolved DOS for the whole Brillouin zone [Fig. 5(c)] further confirm the quantization and localization of the xz- and yz-based bulk states and the presence of unaffected itinerant bonding xy

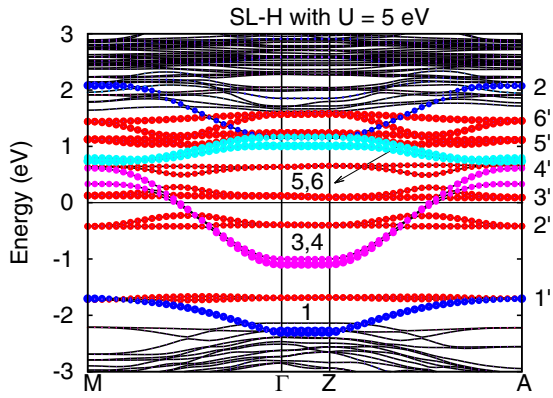

FIG. 6. The planar xy projected bands (1 to 6) and z-axis-oriented xz- and yz-orbital projected bands (1′ to 6′) in the spin-down channel for the SL-H superlattice. The results are obtained for $U = 5\,\text{eV}$.

states. The charge density plot of Fig. 5(d) provides a visualization assessment of the orbital contribution of bands 3, 4, 2′, and 3′.

To examine the robustness of the quantization and the 2DEG, we have examined the ground-state electronic structure of the lower-symmetry structure [SL-L, Fig. 1(b)], where the SL is designed assuming the SL is grown on a LCMO substrate. Also, the electronic structure of an intermediate symmetry (SL-I), designed by taking the average of the LCMO and SFMO crystals, is calculated. Figures 5(e) and 5(f) show the spin-down band structure of the SL-I and SL-L configurations. While the crystal structure of SL-H is tetragonal, it is monoclinic for SL-I and SL-L. With lowering the symmetry from tetragonal to monoclinic ($\beta \neq 90^\circ$), there is an intermixing of the xy state with the xz and yz states through intersite hybridization. This results in discretization and minor localization of the planar xy-dominated bands, as can be observed from Figs. 5(e) and 5(f). However, the effect is very weak and can be neglected. Later (in Fig. 7 below), we will find that the electrical conductivity along the superlattice growth direction is negligible for all the superlattices, confirming the electron conduction confined to the xy plane.

To see if the spin-polarized 2DEG and the quantized states remain invariant with respect to the strong correlation effect, we have further examined the electronic structure for higher values of U. The spin-down band structure of the SL-H superlattice for $U = 5\,\text{eV}$ is shown in Fig. 6. We find that the formation of 2DEG is invariant. However, a higher value of U further localizes the quantized states. In Appendix C, we apply different U to different transition elements and still find that it has no bearing on the formation of 2DEG.

VI. TRANSPORT PROPERTIES

The formation of a spin-polarized 2DEG out of a bulk SFMO 3DEG through the confinement effect can be quantified by calculating the conductivity. For this, we have adopted semiclassical Boltzmann transport theory as implemented in the BOLTZTRAP code [33] and calculated the conductivity tensor σ from the first-order derivatives of the bands $\epsilon(k)$:

$$\sigma_{\alpha\beta}(\epsilon) = \frac{e^2\tau}{N}\sum_{i,\mathbf{k}} v_\alpha(i,\mathbf{k})v_\beta(i,\mathbf{k})\frac{\delta(\epsilon-\epsilon_{i,\mathbf{k}})}{d\epsilon}, \qquad (3)$$

where τ is the relaxation time, i is the band index, v is the first- order derivative of $\epsilon_{i,\mathbf{k}}$, and N is the number of $\mathbf{k}$ points sampled. The notations α and β stand for the crystal axes. The temperature-dependent conductivity as evaluated using Eq. (3) is

$$\sigma_{\alpha\beta}(T,\mu) = \frac{1}{\Omega}\int \sigma_{\alpha\beta}(\epsilon)\Big[-\frac{\partial f_\mu(T,\epsilon)}{\partial\epsilon}\Big]d\epsilon, \qquad (4)$$

where Ω is the volume of the unit cell, $\mu(=E_F)$ is the chemical potential, and f is the Fermi-Dirac distribution function.

In Fig. 7, we plot σ/τ vs $E - E_F$ at room temperature for both the bulk and superlattices. In bulk SFMO, conductivity along all three principal axes is nearly the same as it has partially occupied dispersive threefold-degenerate t_{2g} states (see Fig. 2). In contrast, for the SL-H superlattice, the potential along z restricts the electronic motion along [001]. Hence, σ_{xx}/τ and σ_{yy}/τ are finite, but σ_{zz}/τ is negligible. However, the magnitude of conductivity along x or y has decreased, approximately by two thirds, compared to the bulk. This decrease is due to the fact that in SL-H, xz and yz orbitals are no longer dispersive. Only the bonding dispersive

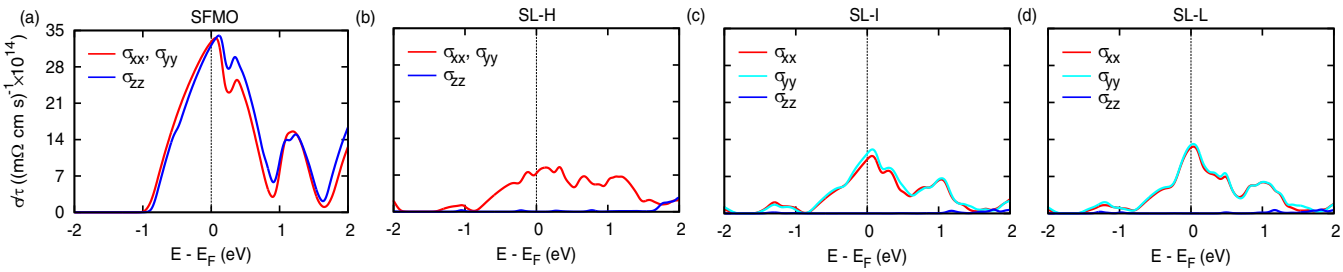

FIG. 7. Transport properties of bulk SFMO and SFMO/LCMO superlattices. The principal component of the electrical conductivity tensor at room temperature for (a) bulk SFMO, (b) SL-H, (c) SL-I, and (d) SL-L superlattices. The results are obtained from Eq. (4) using semiclassical Boltzmann transport theory. The confinement potential restricts the electron motion along [001], and hence, σ_{zz} becomes negligible. Significant values of σ_{xx} and σ_{yy} imply two-dimensional mobility of the electrons, and hence, the formation of a spin-polarized 2DEG. Due to xy planar symmetry, σ_{xx} and σ_{yy} are the same in bulk SFMO and the SL-H superlattice. Minor distortion in the plane makes them distinguishable in the SL-I and SL-L superlattices.

band dominated by the planar xy orbital contributes to the conductivity. The σ/τ vs $E - E_F$ plot for the SL-I and SL-L superlattices with reduced symmetry also shows conductivity phenomena similar to that of SL-H, suggesting the robustness of the spin-polarized 2DEG against any perturbation through lattice distortion.

VII. CONCLUSIONS

In summary, using the DFT+U method, we have shown that a magnetic metal-insulator superlattice Sr_2FeMoO_6/La_2CoMnO_6 creates a spin-polarized 2DEG (SP-2DEG). Our study provides an alternate quantization mechanism to intrinsically form 2DEG which is very different from the conventional engineering of polar heterointerfaces to achieve the same. The quantization mechanism involves confinement of the spin-polarized mobile electrons through a periodic finite square-well potential and further localization of the quantized states through the strong correlation effect. This restricts the mobility of the electron gas to the plane perpendicular to the potential well. An experimental realization of such a superlattice will be an ideal platform to study several fundamental phenomena like the intrinsic anomalous Hall effect and the Rashba effect. Since the bulk magnetic order is unaffected in this superlattice, it is expected to have a high Curie temperature as in the bulk. Therefore, the SP-2DEG formed here will be useful for spintronic applications.

ACKNOWLEDGMENTS

The authors would like to thank HPCE, IIT Madras, for providing the computational facility. This work is supported by the Department of Science and Technology, India, through Grant No. EMR/2016/003791.

APPENDIX A: MECHANISM OF HALF-METALLIC BEHAVIOR IN Sr_2FeMoO_6 AND INSULATING BEHAVIOR IN La_2CoMnO_6

The spin-resolved total and partial DOSs in Fig. 8(a), obtained with DFT and DFT+U, describe the bulk electronic structure of Sr_2FeMoO_6 and La_2CoMnO_6. Figure 8(b) schematically illustrates the mechanism responsible for the half-metallic behavior of Sr_2FeMoO_6 and the insulating behavior of La_2CoMnO_6.

In a nonmagnetic configuration, half-filled $3d$ states of Fe^{3+} and partially occupied $4d$ states of Mo^{5+} create a high DOS at E_F to make the system unstable, and the system becomes stable through spin polarization. Now with large spin-exchange splitting, the Fe d states are occupied in the spin-up channel and are empty in the spin-down channel. However, there is a larger overlap between the Fe t_{2g} and Mo t_{2g} spin-down bands, which leads to a stronger hybridization between these two, where the bonding band is more predominantly occupied by the Mo t_{2g} states. This creates a sort of negative exchange splitting [41,42].

The compound LCMO is a correlated insulator. In the absence of any lattice distortion and strong on-site correlation effect, LCMO is half metallic within GGA. Due to the distorted CoO_6 octahedra, there is a partial removal of the threefold degeneracy of the t_{2g} states, which gives rise to a pseudogap at E_F [37]. However, with the inclusion of on-site correlation U, a gap is opened up in the spin-down channel by splitting the Co t_{2g} state into the lower Hubbard band and the upper Hubbard band.

With the formation of the superlattice, following the steps proposed in Fig. 1(c), the bulk xz and yz states are quantized, leaving the partially occupied dispersive spin-down xy states of SFMO unchanged, and finally form the 2DEG. This is reflected in the superlattice DOS plotted in Fig. 8(c).

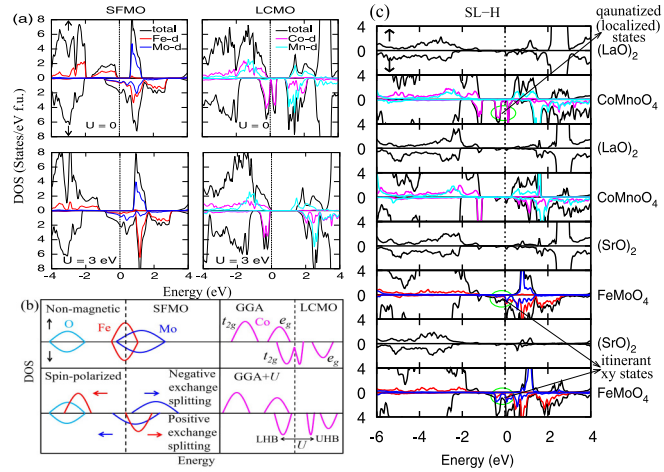

FIG. 8. (a) Spin-resolved total and partial densities of states of bulk SFMO and LCMO. For SFMO, the gap in the spin-up channel exists even without the strong correlation effect. The partially occupied dispersive Fe-Mo t_{2g} hybridized bonding state makes the spin-down channel conducting. Within GGA, ferromagnetic LCMO is insulating in the spin-up channel, and it exhibits a pseudogap at E_F in the spin-down channel. With inclusion of strong on-site correlation, the real gap opens up to make the system insulating. (b) Schematic illustration of the mechanism that makes SFMO half metallic and LCMO insulating. (c) Layer-resolved total and partial DOSs for the $(SFMO)_2/(LCMO)_2$ SL-H superlattice. These layer-resolved DOSs replicate the bottom panel of Fig. 1(c).

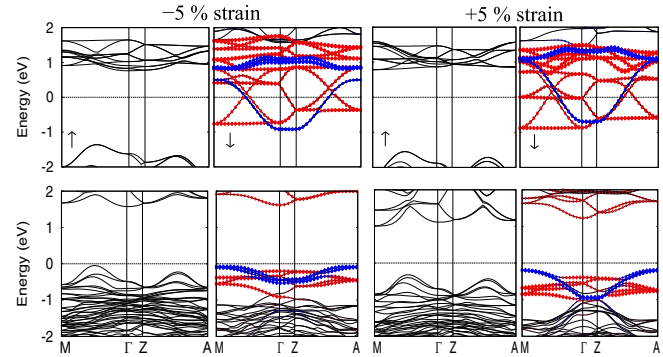

FIG. 9. (GGA + U; $U = 3$ eV) Spin-polarized band structure of bulk SFMO (top panel) and LCMO (bottom panel) in the presence of compressive and tensile strain. The results are obtained using a four-formula unit cell. The color code is the same as in Fig. 4.

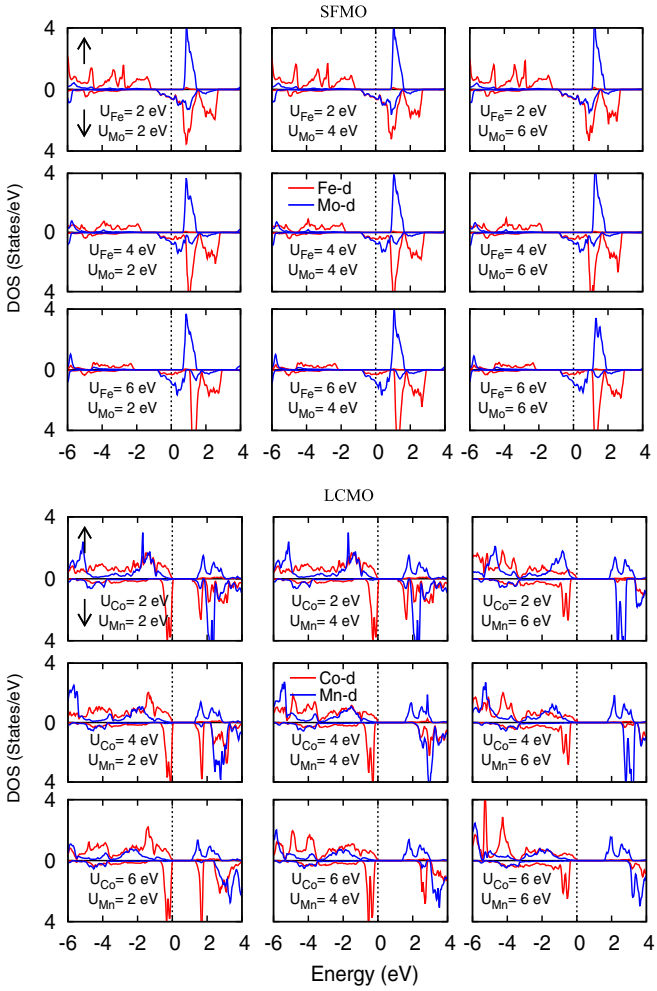

FIG. 10. GGA+U spin-polarized partial densities of states for bulk SFMO (top panel) and LCMO (bottom panel). Different U values have been considered for different transition-metal elements. Irrespective of U values, SFMO and LCMO retain their half-metallic and insulating behavior, respectively.

APPENDIX B: EFFECT OF STRAIN ON BULK COMPOUNDS

Superlattices grown on substrates experience epitaxial strain which can influence their electronic structure. In this regard examining the strain effect on the respective bulk compounds is a good starting point. In Fig. 9, we show the bulk band structure of SFMO and LCMO in the presence of ±5% epitaxial strain. We find that irrespective of the nature of strain, compressive or tensile, both of the compounds are insulating in the spin-up channel akin to the unstrained condition. The spin-down channel, which is responsible for the eigenstate reconstruction to create the 2DEG, also retained the metallic and insulating behaviors of SFMO and LCMO, respectively. In fact, there is no change in the shape of the band dispersion, except for a minor variation in the bandwidth. Hence, it can be inferred that in the absence of the extreme strain condition, the 2DEG formation in the $(SFMO)_2/(LCMO)_2$ superlattice will remain invariant.

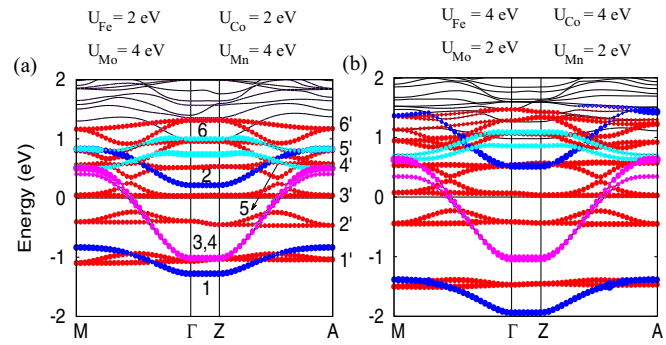

FIG. 11. Spin-down band structure of the SL-H superlattice obtained using two different sets of U values as indicated. Here, we infer that the formation of a 2DEG is an invariant phenomenon in this superlattice. The color code is the same as in Fig. 4.

APPENDIX C: INVARIANCE OF BULK AND SUPERLATTICE ELECTRONIC STRUCTURES WITH DIFFERENT U

Since both LCMO and SFMO are strongly correlated oxides, it is expected that the on-site repulsion U will have a major role in determining their ground-state electronic structures. In the main text, we discussed the results with same value of U (3 and 5 eV) for Co, Mn, Fe, and Mo. However, in general U is different for different elements. In this Appendix, we report whether the salient features of the bulk and superlattice electronic structures of these double perovskites remain the same even if different U values are used. In Fig. 10, we plot the Fe d and Mo d DOSs for SFMO and Mn d and Co d DOSs for LCMO for different pairs of U values for each of them. We find that the half-metallic nature of SFMO and the insulating nature of LCMO are not affected. However, there is a minor redistribution of the states around the Fermi level. Such a redistribution causes a minor change in the occupancy of the d states for the half-metallic system. The spin-down band structures plotted in Fig. 11 suggest that the formation of a 2DEG in the $(SFMO)_2/(LCMO)_2$ superlattice and the quantization of the states, as discussed in the main text, are universal and are not affected by the change in U values. However, as expected, the band centers of the lower and upper Hubbard bands vary with U.

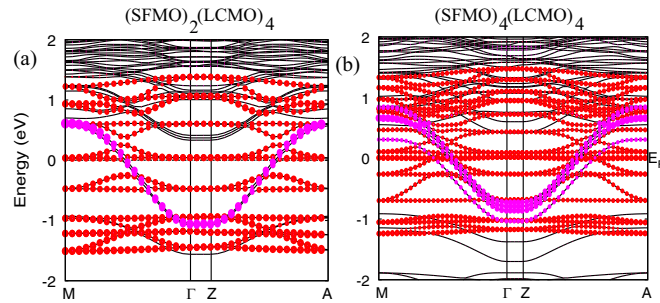

FIG. 12. The spin-down band structure of (2,4) and (4,4) SFMO/LCMO superlattices. The calculations are carried out with $U = 3$ eV on a relaxed structure. The color code is the same as in Fig. 4.

APPENDIX D: EFFECT OF THE SUPERLATTICE PERIOD

As the eigenstate reconstruction of this superlattice depends on the potential profile of the system (see Fig. 3), it is expected that the period of the superlattice will influence its electronic structure. With this objective, in Fig. 12, we plot the band structures of the $(SFMO)_2/(LCMO)_4$ and $(SFMO)_4/(LCMO)_4$ superlattices. We find that the itinerant behavior of the xy-dominated bands is not affected by the superlattice period. However, although xz- and yz-dominated bands are discretized, the extent of localization of these states is affected by the thickness of SFMO. With increasing thickness, the electron localization along the superlattice growth direction reduces, which weakens the formation of the spin-polarized 2DEG. However, this is a preliminary study, and a detailed in-depth study is required to have better understanding of the effect of the superlattice period on the electronic structure.

[1] Y. Cui and C. M. Lieber, Science **291**, 851 (2001).
[2] R. G. Mani, J. H. Smet, K. von Klitzing, V. Narayanamurti, W. B. Johnson, and V. Umansky, Nature (London) **420**, 646 (2002).
[3] L. Nádvorník, P. Němec, T. Janda, K. Olejník, V. Novąk, V. Skoromets, H. Němec, P. Kužel, F. Trojánek, T. Jungwirth, and J. Wunderlich, Sci. Rep. **6**, 22901 (2016).
[4] K. Yoshimatsu, K. Horiba, H. Kumigashira, T. Yoshida, A. Fujimori, and M. Oshima, Science **333**, 319 (2011).
[5] H. Y. Hwang, Y. Iwasa, B. Kawasaki, M. Keimer, N. Nagaosa, and Y. Tokura, Nat. Mater. **11**, 103 (2012).
[6] E. Dagotto, Science **309**, 257 (2005).
[7] J. Chakhalian, J. W. Freeland, A. J. Millis, C. Panagopoulos, and J. M. Rondinelli, Rev. Mod. Phys. **86**, 1189 (2014).
[8] A. Ohtomo and H. Y. Hwang, Nature (London) **427**, 423 (2004).
[9] N. Nakagawa, H. Y. Hwang, and D. A. Muller, Nat. Mater. **5**, 204 (2006).
[10] K. Janicka, J. P. Velev, and E. Y. Tsymbal, Phys. Rev. Lett. **102**, 106803 (2009).
[11] A. Bhattacharya, S. J. May, S. G. E. te Velthuis, M. Warusawithana, X. Zhai, B. Jiang, J.-M. Zuo, M. R. Fitzsimmons, S. D. Bader, and J. N. Eckstein, Phys. Rev. Lett. **100**, 257203 (2008).
[12] B. R. K. Nanda and S. Satpathy, Phys. Rev. Lett. **101**, 127201 (2008).
[13] Z. Wan, A. Kazakov, M. J. Manfra, L. N. Pfeiffer, K. W. West, and L. P. Rokhinson, Nat. Commun. **6**, 7426 (2015).
[14] M. Kjaergaard, F. Nichele, H. J. Suominen, M. P. Nowak, M. Wimmer, A. R. Akhmerov, J. A. Folk, K. Flensberg, J. Shabani, C. J. Palmstrøm, and C. M. Marcus, Nat. Commun. **7**, 12841 (2016).
[15] Y. Tokura, Phys. Today **56**(7), 50 (2003).
[16] Y. Tokura and N. Nagaosa, Science **288**, 462 (2000).
[17] K.-I. Kobayashi, T. Kimura, H. Sawada, K. Terakura, and Y. Tokura, Nature (London) **395**, 677 (1998).
[18] R. P. Panguluri, S. Xu, Y. Moritomo, I. V. Solovyev, and B. Nadgorny, Appl. Phys. Lett. **94**, 012501 (2009).
[19] R. I. Dass and J. B. Goodenough, Phys. Rev. B **67**, 014401 (2003).
[20] C. L. Bull, D. Gleeson, and K. S. Knight, J. Phys.: Condens. Matter **15**, 4927 (2003).
[21] C. Du, R. Adur, H. Wang, A. J. Hauser, F. Yang, and P. C. Hammel, Phys. Rev. Lett. **110**, 147204 (2013).
[22] A. J. Hauser, R. E. A. Williams, R. A. Ricciardo, A. Genc, M. Dixit, J. M. Lucy, P. M. Woodward, H. L. Fraser, and F. Yang, Phys. Rev. B **83**, 014407 (2011).
[23] R. Galceran, L. López-Mir, B. Bozzo, J. Cisneros-Fernández, J. Santiso, L. Balcells, C. Frontera, and B. Martínez, Phys. Rev. B **93**, 144417 (2016).
[24] M. N. Iliev, M. V. Abrashev, A. P. Litvinchuk, V. G. Hadjiev, H. Guo, and A. Gupta, Phys. Rev. B **75**, 104118 (2007).
[25] C.-I. Li, J.-C. Lin, H.-J. Liu, M.-W. Chu, H.-W. Chen, C.-H. Ma, C.-Y. Tsai, H.-W. Huang, H.-J. Lin, H.-L. Liu, P.-W. Chiu, and Y.-H. Chu, Chem. Mater. **28**, 3914 (2016).
[26] P.-C. Wu, P.-F. Chen, T. H. Do, Y.-H. Hsieh, C.-H. Ma, T. D. Ha, K.-H. Wu, Y.-J. Wang, H.-B. Li, Y.-C. Chen, J.-Y. Juang, P. Yu, L. M. Eng, C.-F. Chang, P.-W. Chiu, L. H. Tjeng, and Y.-H. Chu, ACS Appl. Mater. Interfaces **8**, 33794 (2016).
[27] J. Jiang, Y. Bitla, C.-W. Huang, T. H. Do, H.-J. Liu, Y.-H. Hsieh, C.-H. Ma, C.-Y. Jang, Y.-H. Lai, P.-W. Chiu, W.-W. Wu, Y.-C. Chen, Y.-C. Zhou, and Y.-H. Chu, Sci. Adv. **3**, e1700121 (2017).
[28] T. Amrillah, Y. Bitla, K. Shin, T. Yang, Y.-H. Hsieh, Y.-Y. Chiou, H.-J. Liu, T. H. Do, D. Su, Y.-C. Chen, S.-U. Jen, L.-Q. Chen, K. H. Kim, J.-Y. Juang, and Y.-H. Chu, ACS Nano **11**, 6122 (2017).
[29] P. Giannozzi *et al.*, J. Phys.: Condens. Matter **21**, 395502 (2009).
[30] P. Blaha, K. Schwarz, G. K. H. Madsen, D. Kvasnicka, and J. Luitz, *WIEN2k: An Augmented Plane Wave Plus Local Orbitals Program for Calculating Crystal Properties* (TU Wien, Vienna, 2001).
[31] J. P. Perdew, K. Burke, and M. Ernzerhof, Phys. Rev. Lett. **77**, 3865 (1996).
[32] S. L. Dudarev, G. A. Botton, S. Y. Savrasov, C. J. Humphreys, and A. P. Sutton, Phys. Rev. B **57**, 1505 (1998).
[33] G. K. Madsen and D. J. Singh, Comput. Phys. Commun. **175**, 67 (2006).
[34] D. D. Sarma, P. Mahadevan, T. Saha-Dasgupta, S. Ray, and A. Kumar, Phys. Rev. Lett. **85**, 2549 (2000).
[35] S. Baidya and T. Saha-Dasgupta, Phys. Rev. B **84**, 035131 (2011).
[36] M. Zhu, Y. Lin, E. W. C. Lo, Q. Wang, Z. Zhao, and W. Xie, Appl. Phys. Lett. **100**, 062406 (2012).
[37] P. Parida, R. Kashikar, A. Jena, and B. R. K. Nanda, J. Phys. Chem. Solids **123**, 133 (2018).
[38] S. Lv, X. Liu, H. Li, L. Han, Z. Wang, and J. Meng, J. Comput. Chem. **33**, 1433 (2012).
[39] A. Franciosi and C. G. V. de Walle, Surf. Sci. Rep. **25**, 1 (1996).
[40] M. Koberidze, A. V. Feshchenko, M. J. Puska, R. M. Nieminen, and J. P. Pekola, J. Phys. D **49**, 165303 (2016).
[41] T. Saitoh, M. Nakatake, A. Kakizaki, H. Nakajima, O. Morimoto, S. Xu, Y. Moritomo, N. Hamada, and Y. Aiura, Phys. Rev. B **66**, 035112 (2002).
[42] B. R. K. Nanda and I. Dasgupta, Comput. Mater. Sci. **36**, 96 (2006).